ELSEVIER

Surface Science 414 (1998) 330–340

surface science

Adsorption of thermal D atoms on Sn/Pt(111) surface alloys

M.R. Voss, H. Busse, B.E. Koel *

University of Southern California, Department of Chemistry, Los Angeles, CA 90089-0482, USA

Received 17 March 1998; accepted for publication 19 May 1998

Abstract

The adsorption of D atoms on Pt(111) and two, well-defined Pt–Sn surface alloys – the p(2×2) Sn/Pt(111) with $\Theta_{Sn}=0.25$ ML and $(\sqrt{3}\times\sqrt{3})R30^\circ$ Sn/Pt(111) with $\Theta_{Sn}=0.33$ ML – has been investigated by using TPD in order to probe the influence of alloyed Sn on Pt–D interactions. Because these alloys do not dissociatively chemisorb room-temperature, ground-state D_2 under UHV conditions, adsorption of thermal D atoms on the alloys was achieved by using a resistively heated Pt tube source operated at 1300 K. Alloying with Sn decreases the saturation coverage of D adatoms from 0.95 ML on the Pt(111) surface to 0.68 and 0.51 ML on the two alloys, respectively, with increasing Sn concentration. The D atom initial sticking coefficient also decreases from 1 to 0.33 to 0.18 in the same series with increasing Sn concentration in these two Pt–Sn surface alloys. Alloying Sn into the Pt(111) surface initially has no effect on the Pt–D bond dissociation energy, D(Pt–D), with D(Pt–D)=252 kJ mol^{-1} on both Pt(111) and the (2×2) alloy, but increasing the surface Sn concentration to 0.33 ML and removing the pure-Pt threefold sites in forming the $(\sqrt{3}\times\sqrt{3})R30^\circ$ alloy causes a 10% decrease in the Pt–D bond energy to 232 kJ mol^{-1}.

Keywords: Adatoms; Alloys; Chemisorption; Deuterium; Hydrogen; Low index single crystal surfaces; Molecule–solid reactions; Platinum; Sticking; Thermal desorption spectroscopy; Tin

1. Introduction

The chemistry of hydrogen at metal surfaces has been the subject of numerous studies [1], largely due to applications in heterogeneous catalysis. Since metal-based catalysts contain several metal components, some fundamental studies have been carried out on the interaction of hydrogen with bimetallic and alloy single crystal surfaces. These systems include $Cu_3Pt(111)$ [2], CuPd(110) [3], CuNi(110) [4], CuRu(111) [5], PdAg(111) [6], AgRu(1010) [7], PtNi(111) [8], PtSn(111) [9], and NiAl(110) [10]. Many of these investigations have selected systems that contain a reactive transition metal (e.g. Pt, Pd, Ru, or Ni) and a noble metal (Cu, Ag, or Au). These surfaces can have a high selectivity for particular hydrocarbon reactions, and the altered chemistry and catalysis has been attributed to either ensemble (geometric) or ligand (electronic) effects [2].

In the Sn/Pt(111) system, we have a nice opportunity to study the chemistry of two closely related surface alloys [11–13] in order to improve our understanding of what controls alloy reactivity. The p(2×2) Sn/Pt(111) surface alloy (referred to hereafter as the (2×2) alloy) has a composition of Pt_3Sn ($\Theta_{Sn}=0.25$ ML) and does not contain any adjacent pure-Pt threefold sites. The $(\sqrt{3}\times\sqrt{3})R30^\circ$ Sn/Pt(111) surface alloy (referred

* Corresponding author. Fax: +1 213 746 4945;
e-mail: koel@cheml.usc.edu

0039-6028/98/$ – see front matter
PII: S0039-6028(98)00429-4

to hereafter as the $\sqrt{3}$ alloy) has a composition of Pt_2Sn ($\Theta_{Sn}=0.33$ ML) and does not have any pure-Pt threefold sites. In addition, Pt–Sn catalysts are used commercially for hydrocarbon reforming [14,15] and selective (de)hydrogenation [16], and so a surface science approach to this catalysis is to explore the chemistry of hydrocarbons and hydrogen on well-defined Pt–Sn surfaces. To this end, we have investigated the adsorption and reaction of a number of small alkanes [17–19], alkenes [20–23], alkynes [24] and arenes [18] on these two surface alloys under UHV conditions.

Hydrogen plays a key role in these hydrocarbon conversion reactions, and its interaction with Pt surfaces has been studied extensively. The dissociative adsorption of H_2 on Pt(111) at 100 K occurs with an initial dissociative sticking coefficient of 0.05 [25,26] with an isosteric heat of adsorption of 67 ± 7 kJ mol^{-1} at low coverage [27]. Hydrogen adatoms on Pt(111) occupy h.c.p. threefold hollow sites [28,29]. The interaction of hydrogen with the Sn/Pt(111) surface alloys is more difficult to study since H_2 dissociative chemisorption does not occur on these surfaces under UHV conditions. By utilizing a clean source of atomic hydrogen, we have now carried out measurements of the adsorption kinetics of D atoms and desorption kinetics of D_2 on these Pt–Sn alloys. These data expand on a brief previous report of molecular and atomic hydrogen adsorption on these surfaces [9], and also complement recent hyperthermal D_2 molecular beam studies [30]. More detailed measurements of hydrogen abstraction rates from these surfaces by incident thermal D(H) atoms will be reported elsewhere [31].

2. Experimental

The experiments were performed in a three-level, stainless-steel UHV ($P_0\leq2\times10^{-10}$ Torr) chamber, which has been previously described [32]. Briefly, in this chamber, we can perform AES, XPS, and UPS using a double-pass CMA, LEED, TPD with a UTI 100C QMS, and HREELS using a LK-2000 spectrometer.

The Pt(111) single crystal (Atomergic; 3 N purity) was cleaned by Ar^+ ion sputtering, oxygen treatments, and annealing. Sample cleanliness was verified by AES and LEED. Sn dosing was performed by resistively heating a Ta boat containing a pure Sn ingot. Formation of the Sn/Pt surface alloys was carried out by deposition of a few monolayers of Sn and subsequent annealing, as described previously [11]. LEED and AES were used to confirm that the alloys were correctly made for each experiment.

A Pt tube doser was constructed, based on the design of Engel and Rieder [33] as a pyrolytic source of hydrogen atoms. The principal component is a bent Pt tube (1 mm O.D., 0.8 mm I.D.) into which a hole of 0.1 mm diameter was mechanically drilled. The tube was resistively heated up to 1275°C, and water cooling kept the adjacent Cu block cold. The temperature of the Pt tube was directly measured by an optical pyrometer that was calibrated by the temperature of the Pt(111) crystal sample, as measured by a Cr/Al thermocouple. The estimated relative accuracy of the pyrometer reading was ±5°C. The flux of D atoms obtained from this source at 1030°C and a chamber pressure of 1×10^{-8} Torr was 2×10^{13} atoms cm$^{-2}\cdot$s^{-1}. This value was obtained by assuming that the initial sticking coefficient of D atoms on Pt(111) at 110 K was unity and that the monolayer saturation coverage of D produced by D_2 exposure on Pt(111) at 110 K was 0.8 ML [34]. This D atom source has the desirable features of a low operating temperature and pressure, and was much cleaner than other W tube or W filament dosers in our hands. The normal operating temperature of the Pt tube doser during these experiments was 1027°C, corresponding to an energy (kT) of $\sim$0.1 eV, although it is known that similarly designed thermal atom sources do not necessarily produce atoms in a Boltzmann energy distribution [35].

D_2 (Cambridge Isotope Labs; 99.7%) and H_2 (Matheson; 99.99%) were introduced via a variable leak valve (Granville-Phillips) into the Pt tube doser. A liquid nitrogen cooled trap was used in the gas inlet lines. Mass spectroscopy performed in the UHV chamber showed no appreciable concentration of impurities in the source gases.

The end of the UTI mass spectrometer used for TPD measurements was capped by a stainless steel flux shield and outfitted with two high transpar-

ency nickel meshes to minimize electron emission (<80 nA) from the ionizer during the experiment [36].

3. Results and discussion

3.1. D_2 and D on Pt(111)

The chemisorption of deuterium molecules and atoms on the clean Pt(111) surface at 110 K was investigated by TPD. Desorption spectra of D_2 for increasing exposures of both D_2 and D atoms are shown in Figs. 1 and 2, respectively. A heating rate of $2\,K\,s^{-1}$ was used in all TPD spectra reported here. The D_2 TPD spectra are independent of the method of forming the D adlayer. The small initial value of 0.05 [25,26] for the D_2 dissociative sticking coefficient requires very large exposures to reach saturation coverage. In both figures, desorption at low coverage occurs at a peak temperature (T_p) of 350 K, decreasing to 290 K approaching saturation. Following D atom adsorption, a shoulder near 270 K is observed at the highest coverages due to increasing lateral repulsive interactions. This behavior is consistent with previous data for H_2 and D_2 on Pt(111) [37]. Two other minor features are noticeable in Figs. 1 and 2. A broad high-temperature desorption feature at 450–500 K arises from defect sites, which amounts to 2% of the D_2 desorption area in these experiments. A small, low-temperature peak at 170 K appeared sometimes at high exposures because of small amounts (<0.1 ML) of coadsorbed D_2O.

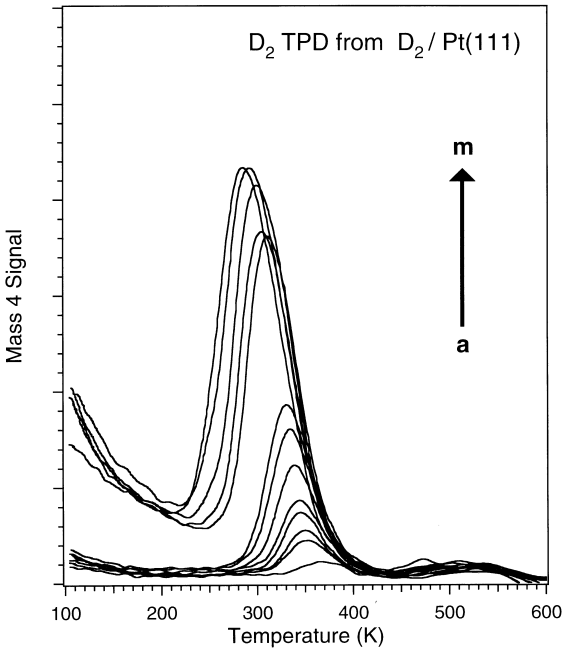

Fig. 1. D_2 TPD spectra after D_2 adsorption on Pt(111) at 110 K. D_2 exposures are from the cold (room temperature) Pt tube doser to give a background pressure of 10^{-8} Torr: (a) 0 L, (b) 0.05 L, (c) 0.10 L, (d) 0.15 L, (e) 0.20 L, (f) 0.40 L, (g) 0.70 L, (h) 1.00 L. Exposures at 10^{-7} Torr: (i) 2.5 L, (j) 5 L, (k) 12.5 L, (l) 125 L, (m) 250 L.

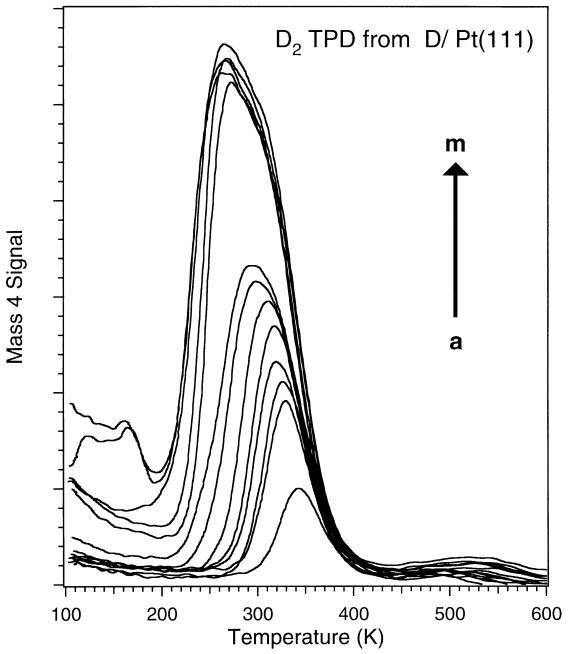

Fig. 2. D_2 TPD spectra after D atom exposures on Pt(111) at 110 K. Relative D atom exposures ($T_{Pt\ tube}=1300$ K) as measured by the D_2 background gas at 10^{-8} Torr: (a) 0 L, (b) 0.05 L, (c) 0.10 L, (d) 0.15 L, (e) 0.20 L, (f) 0.40 L, (g) 0.70 L, (h) 1.00 L. Exposures at 10^{-7} Torr: (i) 2.5 L, (j) 5 L, (k) 12.5 L, (l) 25 L, (m) 50 L.

3.2. D on the p(2×2) Sn/Pt(111) surface alloy

Several large exposures (up to 100 L) of D_2 were made on the (2×2) alloy. Consistent with that

previously reported [9], adsorption of D_2 does not occur on this surface. D_2 thermal desorption spectra following D atom exposures on the (2×2) alloy are reported in Fig. 3. At low exposures of D atoms, desorption occurs at a peak temperature of 371 K, decreasing to 336 K approaching saturation coverage. A low-temperature peak also evolves at about 200 K at the highest coverages. The high-temperature peak can be assigned to adsorption at threefold sites involving three Pt atoms. We ascribe the slightly higher T_p to the influence of an activation barrier to D_2 adsorption present on the Pt–Sn alloy but not on the Pt(111) surface. The low-temperature peak corresponds either to the population of new Pt binding site, such as twofold Pt bridging or Pt atop sites, or to D adsorption at a site influenced directly by Sn, perhaps a threefold site with two Pt atoms and one Sn atom. This low-temperature peak in Fig. 3 is clearly not a D_2O artifact because we observed D_2O desorption only at $T_p=161$ K, well below the observed D_2 desorption peak.

The D_2 desorption spectra in Fig. 3 agree quite well with those in Refs. [9,30], the only exception being the low-temperature D_2 desorption in Fig. 3 at 200 K. It is possible that this represents a true difference in the three experiments, and this state is only populated at high coverages produced from an intense D atom source, but this feature may also arise from unalloyed Sn at the surface in our experiment (vide infra).

3.3. D on the $(\sqrt{3}\times\sqrt{3})R30^\circ$ Sn/Pt(111) surface alloy

The $\sqrt{3}$ alloy was prepared by the evaporation of additional Sn onto the (2×2) alloy and annealing [11]. The TPD results for D_2 desorption following the adsorption of D atoms on the $\sqrt{3}$ alloy are shown in Fig. 4. Desorption at low initial

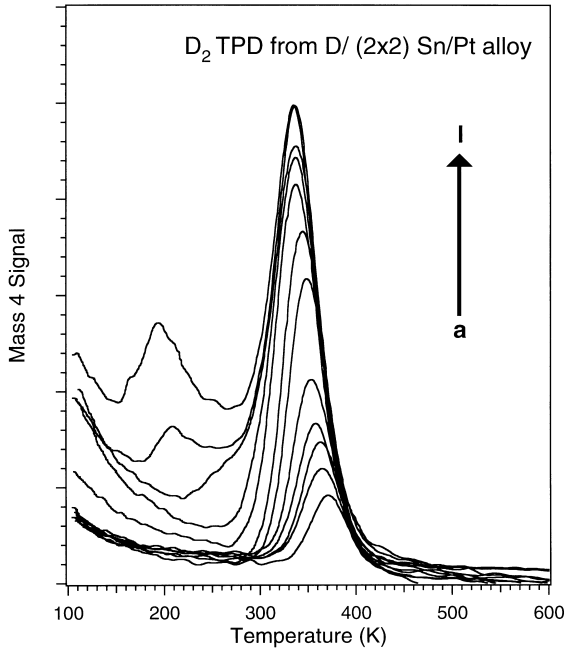

Fig. 3. D_2 TPD spectra after D adsorption on the p(2×2) Sn/Pt(111) surface at 110 K. Exposures at 10^{-8} Torr: (a) 0.05 L, (b) 0.10 L, (c) 0.15 L, (d) 0.20 L, (e) 0.40 L, (f) 0.70 L, (g) 1.00 L. Exposures at 10^{-7} Torr: (h) 1.3 L, (i) 2.6 L, (j) 6.5 L. Exposures at 10^{-6} Torr: (k) 26 L, (l) 130 L.

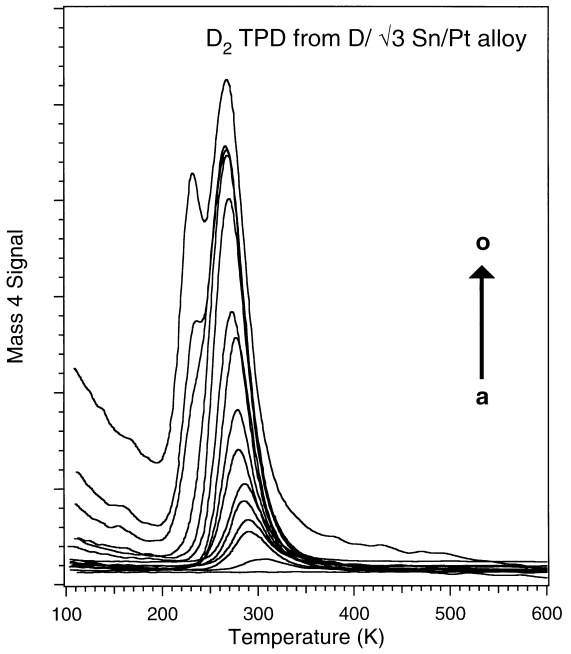

Fig. 4. D_2 TPD spectra after D adsorption on the $(\sqrt{3}\times\sqrt{3})$ R30° Sn/Pt(111) surface at 110 K. Exposures at 10^{-8} Torr: (a) 0 L, (b) 0.01 L, (c) 0.05 L, (d) 0.10 L, (e) 0.15 L, (f) 0.20 L, (g) 0.40 L, (h) 0.70 L, (i) 1.00 L. Exposures at 10^{-7} Torr: (j) 1.3 L, (k) 2.6 L, (l) 6.5 L, (m) 13 L, (n) 26 L. Exposures at 10^{-6} Torr: (o) 65 L.

coverage occurs at 308 K in a peak that shifts to 267 K with increasing coverage. Upon saturation of the first peak, a second peak at 232 K evolves at high exposures. (The tiny desorption near 160 K arises from D_2O coadsorption, and this peak coincides exactly with D_2O desorption after D_2O adsorption on this surface.) The $\sqrt{3}$ alloy exhibits a marked difference in the surface-D interaction that is likely due to the absence of the favored threefold pure-Pt sites that are present on both Pt(111) and the (2×2) alloy. The D atom coverage decreases from 0.95 ML on Pt(111) to 0.68 and 0.51 ML on the two alloys, respectively.

The spectra in Fig. 4 agree well with those in Ref. [30], but are different from those in a former report [9]. We believe that this indicates a better preparation of the $\sqrt{3}$ alloy in the latter cases. Most notably, the high-temperature peak in Ref. [9] corresponds closely to H_2 desorption from the (2×2) Sn/Pt(111) surface, which indicates that a surface was formed with mixed domains of both (2×2) and $\sqrt{3}$ alloys.

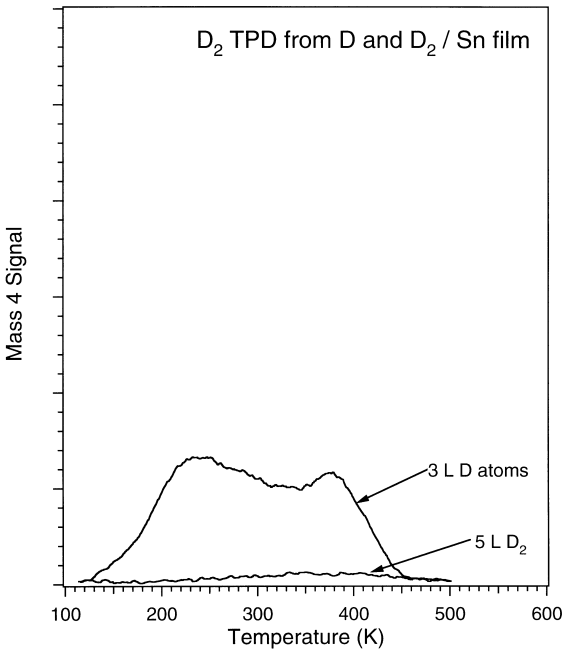

Fig. 5. D_2 TPD spectra after exposures of D_2 (bottom curve) and D atoms (top curve) on a thin S film at 110 K.

3.4. D on a Sn film

A Sn overlayer was prepared by evaporative deposition of Sn on the (2×2) alloy surface at 300 K, followed by annealing to 500 K. The average thickness of this film can be estimated to be 3 ML by AES, assuming a layer-by-layer growth mode of Sn for attenuating the Pt signal. Sn grows on Pt(111) between 140 and 400 K in an ordered structure up to 0.6 ML, and then forms three-dimensional islands [11]. Islanding after completion of the first 2 ML has also been observed at 300 K for Sn on Ni(111) [38] and Pd(111) [39]. We observed a $c(4\times2)$ LEED pattern at low Sn coverages on the (2×2) alloy after annealing to 500 K, but a weak (2×2) alloy pattern for thicker Sn films, in agreement with Ref. [11].

D_2 TPD spectra following exposures of D and D_2 on the Sn overlayer at 110 K are shown in Fig. 5. No molecular chemisorption occurs on the Sn film, as shown in the curve following 5 L D_2 exposure. Adsorption occurs from 3 L exposure of D atoms, and subsequent TPD shows a broad D_2 desorption profile with peaks near 233 and 376 K. The disorder in the deposited Sn film could contribute to the large width of the desorption feature. The large D coverage indicated by the TPD peak area means that adsorbed D atoms are for the most part bonded to Sn atoms. In fact, Sn–H bonds have been observed for a long time in inorganic chemistry. Notably, the first bond dissociation energy, D(Sn–H), in stannane (SnH_4) is 307 kJ mol^{-1} [40], which is larger than the strength of the surface Pt–H bond on Pt(111) where D(Pt–H) = 252 kJ mol^{-1} [37]. This means that D adsorption in the (2×2) and $\sqrt{3}$ alloys might occur at mixed sites involving both Sn and Pt. However, Janin and coworkers [41] assert by high-resolution core level electron spectroscopy that atomic hydrogen bonds only to Pt atoms on the $(\sqrt{3}\times\sqrt{3})$R30° Sn/Pt(111) alloy.

3.5. D adsorption kinetics

Using the D_2 TPD data from Figs. 2–4, we can explore the adsorption kinetics of incident thermal D atoms on Pt(111) and the two Pt–Sn surface alloys at 110 K. Fig. 6 shows the initial uptake of

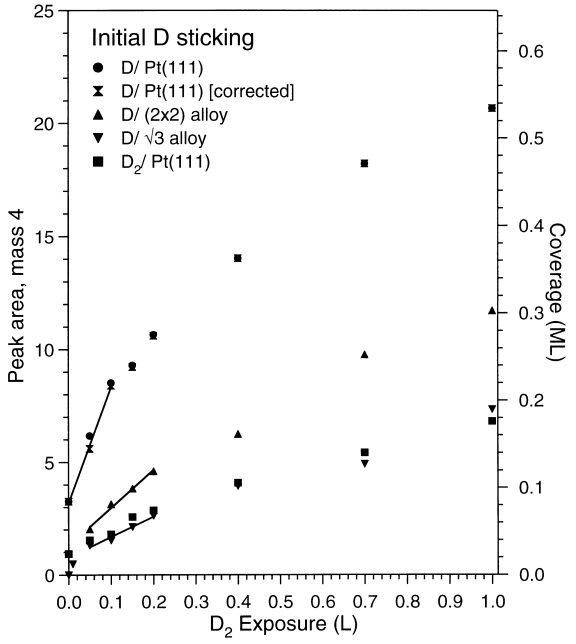

Fig. 6. Adsorbed D uptake curve from integrating the D_2 TPD in the low coverage range. Values for the initial sticking coefficients S_o of D atoms on each surface were obtained by fitting a straight line to the low coverage data for $\Theta_D > 0.05$ ML.

D atoms for the three surfaces derived from the integrated D_2 TPD spectra obtained at low coverages. An absolute coverage scale can be determined by normalizing to $\Theta_D = 0.8$ ML [37] for a saturation D coverage on Pt(111) obtained in our chamber from a 50 L D_2 exposure via a microcapillary array doser. This dosing technique yielded a larger value of Θ_D than in Fig. 1 because of the higher doser enhancement factor and reduced effects from background contamination.

D atom adsorption occurs most readily on the clean Pt(111) surface, and decreases with increasing alloyed Sn concentration. On the alloys, since no D_2 dissociative sticking occurs, the D atom sticking coefficient can be evaluated directly and at near zero coverage. However, a correction must be made to the D/Pt(111) curve from D_2 adsorption because the efficiency of the D atom source is much less than unity. Also, our dosing procedure was to establish a steady-state D_2 gas pressure prior to moving the sample into line-of-sight of the D atom source, which allowed some D_2 adsorption from the background on Pt(111) prior to D atom dosing. Therefore, the data for D atom uptake on Pt(111) were corrected (isosterically) for the adsoprtion of D_2 by using the D_2 molecular uptake curve obtained via the unheated D atom source (shown also in Fig. 6).

The initial sticking coefficients for incident D atoms were obtained by a linear least-squares fit to the data points at the lowest three or four exposures that produced coverages above 0.02 ML (in order to reduce defect contributions). These fits are shown as solid lines in Fig. 6. The relative initial sticking coefficients decrease in a ratio of 1:0.33:0.18, comparing Pt(111) to the (2×2) and $\sqrt{3}$ alloys, respectively. Assuming that the initial sticking coefficient for D atoms on Pt(111) at 110 K is unity leads to values for the D sticking coefficient on the two alloy surfaces of 0.33 and 0.18, as summarized in Table 1. One final observation is that the D atom uptake curves on all three surfaces are curved over most of the coverage range. This means that either a D atom precursor state is not very important to the adsorption kinetics or that there is a significant rate of D atom abstraction occurring from the surface at high coverages. In a separate paper, we will address the D atom abstraction kinetics from the two alloy surfaces [29].

Fig. 7 contains the complete uptake plots showing D atom exposures up to saturation coverages on all three surfaces. The solid curves are given as a guide to the eye only. The saturation coverage of D atoms depends on the concentration of Sn alloyed in the surface, decreasing from 0.95 ML on Pt(111) to 0.68 and 0.51 ML on the two alloys, respectively.

The influence of Sn on the D atom initial sticking coefficient and saturation coverage is quantified in Fig. 8. Based on the results of Ref. [41] discussed

Table 1
D atom sticking coefficients on Sn/Pt(111) surfaces

Surface	S_0
Pt(111)	$\equiv 1$
(2×2) Sn/Pt alloy	0.33 ± 0.1
$\sqrt{3}$ Sn/Pt alloy	0.18 ± 0.1

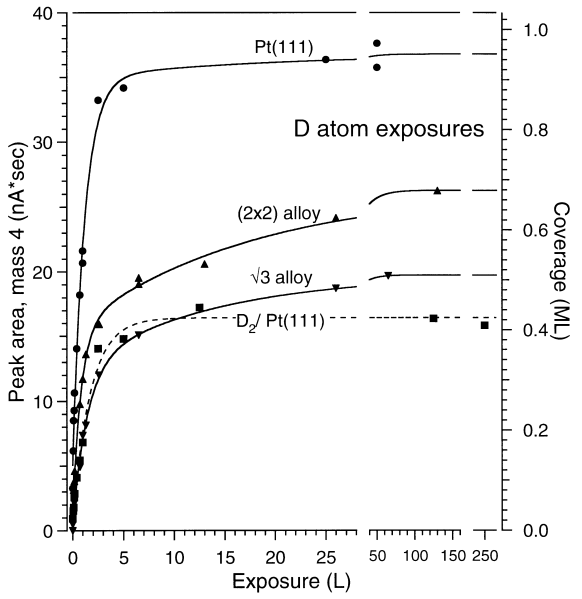

Fig. 7. Adsorbed D uptake curves over the full coverage range, showing the saturation coverages of adsorbed D on the three surfaces. As a reference, the adsorbed D uptake curve (dashed line) from D_2 exposures on Pt(111) at 110 K is also shown.

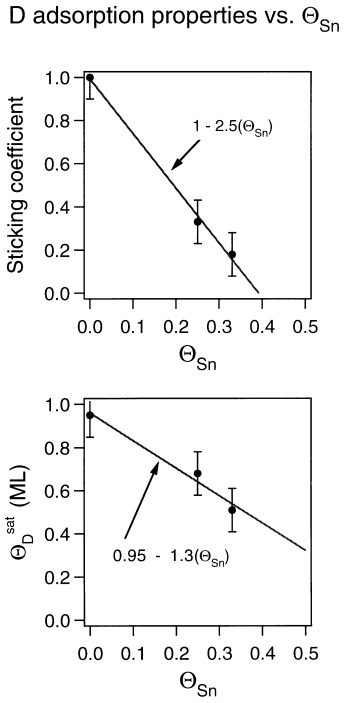

Fig. 8. Influence of alloyed Sn surface atoms on the uptake kinetics for incident D atoms compared to values on Pt(111). Top: initial sticking coefficient, S_o. Bottom: saturation coverage of adsorbed D, Θ_D^{sat}.

above, the lower initial sticking coefficient and saturation coverage of D adatoms on the alloys can be interpreted as due to a site-blocking effect by Sn. The solid curves shown in both panels are fits to the data for a function of the form $(1-a\Theta_{Sn})$, which is expected for Langmuirian adsorption requiring a single site and each Sn atom blocking a sites. Surface Sn has a greater effect on the sticking coefficient, blocking ~ 2.5 sites, than it does on the adsorption sites, blocking these sites nearly 1:1.

A useful comparison of the D_2 TPD curves at saturation D coverage for all of the surfaces that we investigated is given in Fig. 9. Forming either alloy completely eliminates D_2 adsorption, and thus the ensembles needed for D_2 dissociation and D adsorption are clearly different. Even though alloying Sn to form the (2×2) alloy decreases the saturation D coverage, surprisingly, the D_2 TPD peak on the (2×2) alloy does not shift appreciably from the low coverage peaks on Pt(111), and in fact T_p increases compared to Pt(111) at saturation coverage. D_2 desorption from the $\sqrt{3}$ alloy occurs in two sharp peaks probably due to two distinct binding sites. One of these sites might be directly involving Sn since D_2 desorption from a Sn film occurs at similar temperatures, although there is no evidence for this in the studies of Janin and coworkers [41].

3.6. D_2 desorption kinetics and energetics

Some work beyond the TPD spectra presented here eventually needs to be carried out, such as heating-rate variation TPD studies or isothermal desorption studies, in order to understand the desorption kinetics better. However, we can make some reasonable estimates of the desorption activation energies (E_{des}) based on our spectra. We used the method of Falconer and Madix [42] to determine values of E_{des}, and furthermore checked that these values could be used to reproduce our measured TPD spectra by computer simulation using

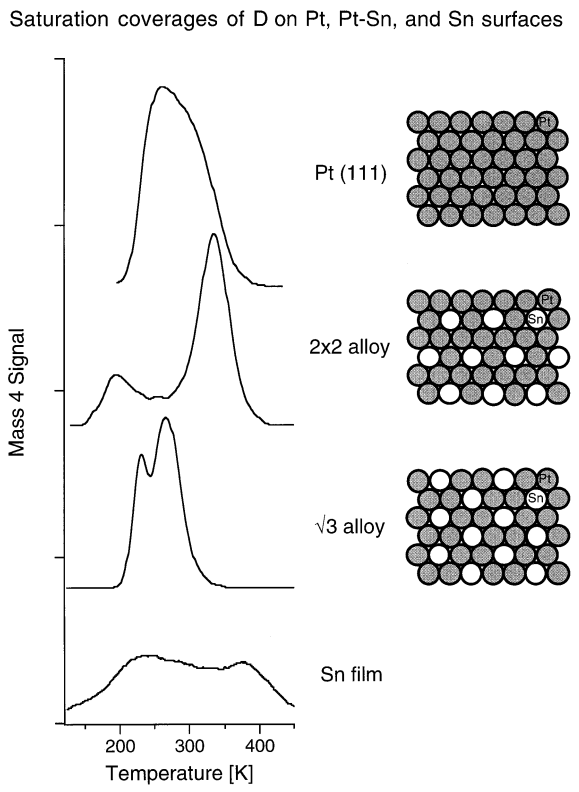

Fig. 9. Comparison of the D_2 TPD spectra obtained for saturation coverages of adsorbed D produced by incident D atoms on several surfaces at 110 K.

the Polanyi–Wigner equation [43,44]

$$\frac{-\mathrm{d}\theta}{\mathrm{d}t} = v\theta^n \exp\left(\frac{-E_{\mathrm{des}}}{RT}\right). \quad (1)$$

The TPD spectra were normalized with respect to coverage, and isothermal plots of $\log(\mathrm{d}\theta/\mathrm{d}t)$ versus $\log\,\theta$ were generated using each set of D_2 desorption spectra for a given substrate in the coverage regime of $\theta_D < 0.4$ ML. The slopes of these isotherms give the order of desorption, n, which we found to be second order. Secondly, isosteres were derived from the isotherms and plotted as $\log(\mathrm{d}\theta/\mathrm{d}t)$ versus $1/T$. The slopes of the isosteres yield E_{des} at a given coverage. On Pt(111), the coverage dependence of E_{des} for $0.5 < \theta_D < 0.3$ ML is reasonably represented by $E_{\mathrm{des}} = 68 - 10\Theta_D)$ kJ mol^{-1}. Such a decrease in E_{des} with increasing coverage can be attributed to weak repulsive interactions in the D adlayer. On the (2×2) and $\sqrt{3}$ alloy, the functions $E_{\mathrm{des}} = (69 - 2\,\theta_D)$ kJ mol^{-1} and $E_{\mathrm{des}} = (55 - 2\theta_D)$ kJ mol^{-1}, respectively, were consistent with the data. The results for E_{des} at $\theta_D = 0$ using these expressions are reported in Table 2. We estimate that the error in these values is less than ± 7 kJ mol^{-1}.

As a check on these values of E_{des}, the measured D_2 TPD spectra (after smoothing and correcting for baseline linearity) were simulated by using $n = 2$ and the above functions for E_{des} in Eq. (1). We varied the value of the preexponential factor (v) to match the experimental data, as shown in Fig. 10. Good fits for all three Pt-containing surfaces were obtained by using $v = 10^{-5}$ cm^2 (atom $\cdot$ s^{-1}). A wide range of values from 3×10^4 [45] to 10^{-2} [46] to 3×10^{-9} [37] have been reported previously for D_2 desorption from Pt(111), and Madix and coworkers have used transition-state theory to ascribe low values of v on platinum surfaces to strong adsorbate–substrate phonon coupling [47]. Attempts by us to use higher or lower values of v caused the peak widths of the simulated peaks to deviate from the measured values over our range of coverages.

Using a simple two-dimensional potential model for the description of the Pt–D interaction, the Pt–D bond dissociation energy, D(Pt–D), can be determined from E_{des} once the activation energy for dissociative D_2 adsorption (E_a^*) is known, as shown in Fig. 11. Recent hyperthermal molecular beam results by Samson et al. [30] estimate values of E_a^* approaching zero on Pt(111) and the (2×2) alloy at 300 K, and $\sim$27 kJ mol^{-1} on the $\sqrt{3}$ alloy. We utilize these values to calculate the values of D(Pt–D) shown in Table 2.

Some of the thermochemistry deduced herein is plotted as a function of surface Sn concentration

Table 2
Thermodynamics of D adsorption on Sn/Pt(111) surfaces (kJ mol^{-1})

Surface	E_{des}	E_a^* [30]	E_{ads}	D(Pt-D)
Pt(111)	68	$\approx$0	68	252
(2×2) Sn/Pt alloy	69	$\approx$0	69	253
$\sqrt{3}$ Sn/Pt alloy	55	$\approx$27	28	232

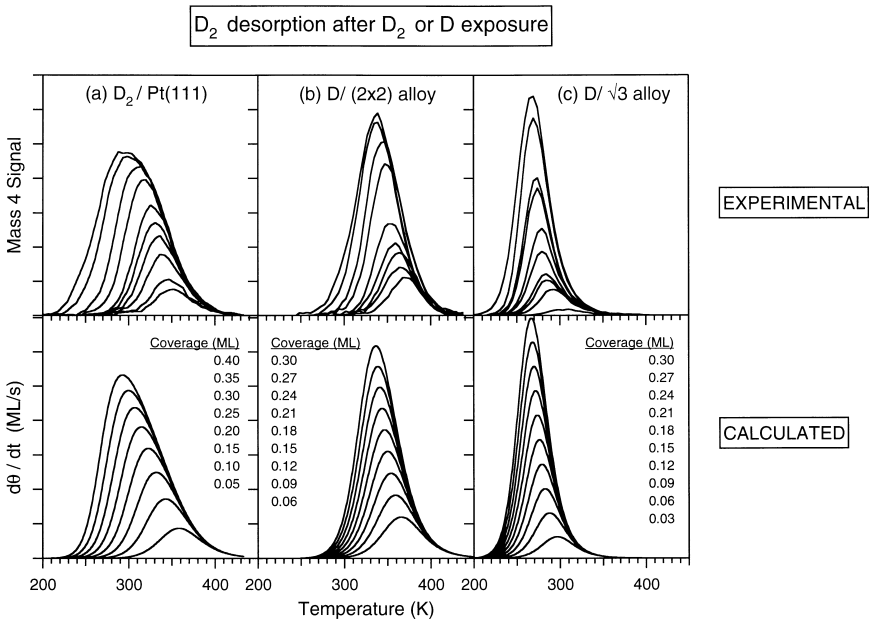

Fig. 10. Experimental (top) and simulated (bottom) TPD spectra for D_2 desorption. Simulation were performed using Eq. (1) with $n=2$.

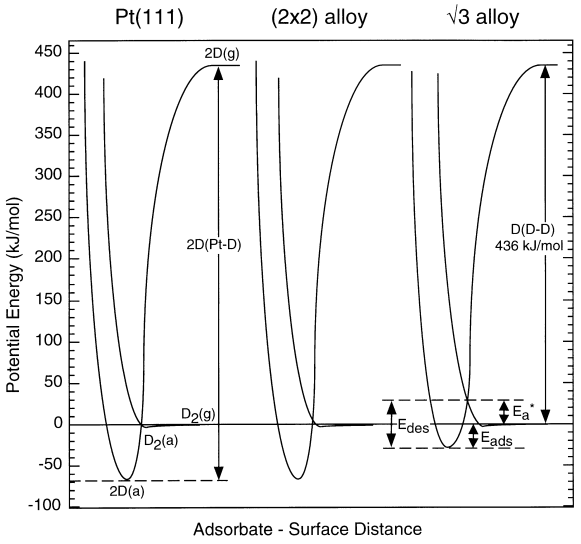

Fig. 11. Two-dimensional potential energy curves for dissociative D_2 chemisorption on Pt(111) and the two ordered surface alloys.

in the alloys in Fig. 12. In the top panel, E_{des} (D_2) first increases slightly from Pt(111) to the (2×2) alloy and then decreases sharply on the $\sqrt{3}$ alloy. As shown in the bottom panel, the Pt–D bond strength remains constant at $\sim 252\ \mathrm{kJ\ mol^{-1}}$ on the Pt(111) and 2×2 alloy surfaces, with the small increase in E_{des} arising from a small increase in E_a^* on this surface. There is a drop in E_{des} to $232\ \mathrm{kJ\ mol^{-1}}$ on the $\sqrt{3}$ alloy, due to a decrease in D(Pt–D). We propose that it is the loss of pure Pt threefold hollow sites that accounts for this decrease in E_{des} (D_2) between the 2×2 and $\sqrt{3}$ alloys. Such data on the Pt–H(D) bond strength are crucially needed for the construction of thermochemical diagrams [48,49] for hydrocarbon conversions reactions on these alloy surfaces.

These results evaluating the energies of the Pt–D bond on the three surfaces are expected to be useful in explaining reactivity and selectivity for hydrocarbon reactions with Pt–Sn catalysts [14–16]. For example, the lifetime of hydrogen adatoms on the (2×2) alloy that may be formed by spillover or dehydrogenation reactions is longer than on a pure Pt(111) surface because of a small increase in the D_2 desorption temperature on this alloy. Our results are also consistent with previous expla-

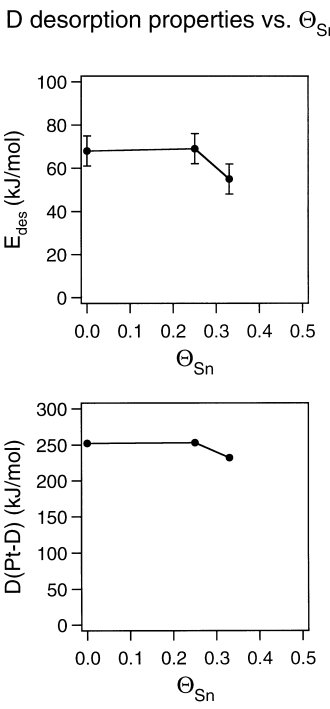

Fig. 12. Influence of alloyed Sn surface atoms on the D_2 desorption energetics (top curve) and Pt–D bond strength (bottom curve) compared to values on Pt(111).

nations of the decreased reactivity of dehydrogenation of ethylene on Sn/Pt alloys [22]. It was concluded that there was an increase in the activation energy for breaking C–H bonds upon alloying with Sn, which was partially ascribed to a decrease in the heat of adsorption of hydrogen. This effect is most pronounced on the $\sqrt{3}$ alloy.

4. Conclusion

We measured the adsorption kinetics of incident thermal D atoms on Pt(111) and two Pt–Sn surface alloys prepared by alloying Sn on Pt(111) to form the p(2×2) Sn/Pt(111) and ($\sqrt{3}\times\sqrt{3}$)R30° Sn/Pt(111) structures. D atom exposures on Pt(111) at 110 K lead to a D coverage of $\Theta_D \sim 0.95$ ML. Alloying Sn with Pt(111) to form these two alloys reduces the uptake of D on the surface. The initial sticking coefficient, S_o, of incident D atoms is reduced linearly by $(1-2.5\Theta_{Sn})$, and the saturation coverage Θ_D^{sat} is reduced by $(1-1.3\Theta_{Sn})$ compared to the Pt(111) surface.

Alloying Sn on Pt(111) to form these surface alloys completely stops dissociative chemisorption of D_2 under UHV conditions. This is a kinetic effect because D adatoms can be readily formed from atomic D exposures. D_2 desorption, for $\Theta_D \sim 0.3$ ML, is characterized by desorption activation energies of $E_{des} = 68$, 69 and 55 kJ mol^{-1} for Pt(111) and the (2×2) and $\sqrt{3}$ surface alloys, respectively. Interestingly, the lifetime of D adatoms, once formed, on the (2×2) alloy is longer than on Pt(111) because of a small increase in the D_2 desorption temperature on this alloy. However, there is a decrease in the D_2 desorption temperature on the $\sqrt{3}$ alloy, and a concomitant decrease in the lifetime of D adatoms because of weakened Pt–D bonding on this surface. We calculate that D(Pt–D) = 252, 253, and 232 kJ mol^{-1} on Pt(111) and the (2×2) and $\sqrt{3}$ surface alloys, respectively. We attribute this weakening to the loss of pure-Pt threefold hollow sites on the $\sqrt{3}$ alloy.

Acknowledgements

We thank J. Küppers and J. Wintterlin for advice in the design and construction of the hydrogen atom doser. We also thank A. Hodgson for valuable discussions and for the preliminary molecular beam results. This work was supported by the Army Research Office and the Division of Chemical Sciences, Office of Basic Energy Sciences, US Department of Energy.

References

[1] K. Christmann, Surf. Sci. Rep. 9 (1988) 1.
[2] U. Schneider, H. Busse, R. Linke, G.R. Castro, K. Wandelt, J. Vac. Sci. Technol. A 12 (1994) 2069.
[3] C. Cottrell, M. Bowker, A. Hodgson, G. Worthy, Surf. Sci. 325 (1995) 57.
[4] K.Y. Yu, D.T. Ling, W.E. Spicer, J. Catal. 44 (1976) 373.
[5] H. Shimizu, K. Christmann, G. Ertl, J. Catal. 61 (1980) 412.
[6] A. Noordermeer, G.A. Kok, B.E. Nieuwenhuys, Surf. Sci. 165 (1986) 375.
[7] P. Lenz, K. Christmann, J. Catal. 139 (1993) 611.

[8] A. Atli, M. Abon, J.C. Bertolini, Y. Boudeville, M. Fallavier, M. Benmansour, J.P. Thomas, J. Phys. Chem. 98 (1994) 4895.
[9] M.T. Paffett, S.C. Gebhard, R.G. Windham, B.E. Koel, J. Phys. Chem. 94 (1990) 6831.
[10] A. Hanbicki, H.L. Davis, A.P. Baddorf, D.B. Poker, E.W. Plummer, Surf. Sci. Lett. 365 (1996) 639.
[11] M.T. Paffett, R.G. Windham, Surf. Sci. 208 (1989) 34.
[12] S.H. Overbury, D.R. Mullins, M.T. Paffett, B.E. Koel, Surf. Sci. 254 (1991) 45.
[13] A. Atrei, U. Bardi, J.X. Wu, E. Zanazzi, G. Rovida, Surf. Sci. 290 (1993) 286.
[14] J.H. Sinfelt, in: J.R Anderson, M. Boudart (Eds.), Catalysis: Science and Technology, Springer, Berlin, 1981, Vol. 1, p. 258.
[15] J.H. Sinfelt, Bimetallic Catalysis: Discoveries, Concepts, and Applications, Wiley, New York, 1983.
[16] R.D. Cortright, J.A. Dumesic, Appl. Catal. A 129 (1995) 101.
[17] C. Xu, B.E. Koel, M.T. Paffett, Langmuir 10 (1994) 166.
[18] C. Xu, Y.L. Tsai, B.E. Koel, J. Phys. Chem. 98 (1994) 585.
[19] C. Xu, B.E. Koel, M.A. Newton, N.A. Frei, C.T. Campbell, J. Phys. Chem. 99 (1995) 16670.
[20] C. Xu, B.E. Koel, Surf. Sci. 304 (1994) 249.
[21] J.W. Peck, B.E. Koel, J. Am. Chem. Soc. 118 (1996) 2708.
[22] Y.L. Tsai, C. Xu, B.E. Koel, Surf. Sci. 385 (1997) 37.
[23] Y.L. Tsai, B.E. Koel, J. Phys. Chem. B 101 (1997) 2895.
[24] C. Xu, J.W. Peck, B.E. Koel, J. Am. Chem. Soc. 115 (1993) 751.
[25] B. Poelsema, L.K. Verheij, G. Comsa, Surf. Sci. 152–153 (1985) 496.
[26] S.C. Gebhard, B.E. Koel, J. Phys. Chem. 96 (1992) 7056.
[27] P.R. Norton, J.A. Davies, T.E. Jackman, Surf. Sci. 121 (1982) 103.
[28] J. Lee, J.P. Cowin, L. Wharton, Surf. Sci. 130 (1983) 1.
[29] K. Mortensen, F. Besenbacher, I. Stensgaard, C. Klink, Surf. Sci. 211–212 (1989) 813.
[30] P. Samson, A. Nesbitt, B.E. Koel, A. Hodgson, J. Chem. Phys., in press.
[31] H. Busse, M.R. Voss, B.E. Koel, J. Chem. Phys., submitted.
[32] A. Sellidj, B.E. Koel, J. Phys. Chem. 97 (1993) 10076.
[33] T. Engel, K.H. Rieder, in: G. Höhler (Ed.), Structural Studies of Surfaces, Springer, Berlin, 1982, Vol. 91, p. 55.
[34] I.P. Batra, J.A. Barker, D.J. Auerbach, J. Vac. Sci. Technol. A 2 (1984) 943.
[35] C.T. Rettner, J. Chem. Phys. 101 (1994) 1529.
[36] C. Xu, B.E. Koel, Surf. Sci. 292 (1993) L803.
[37] K. Christmann, G. Ertl, T. Pignet, Surf. Sci. 54 (1976) 365.
[38] K. Gürtler, K. Jacobi, Surf. Sci. 134 (1983) 309.
[39] A.F. Lee, C.J. Baddeley, M.S. Tikhov, R.M. Lambert, Surf. Sci. 373 (1997) 195.
[40] L. May, C.R. Dillard, J. Chem. Phys. 34 (1961) 694.
[41] E. Janin, M. Björkqvist, T.M. Grehk, M. Göthelid, C.-M. Pradier, U.O. Karlsson, A. Rosengren, Appl. Surf. Sci. 99 (1996) 371.
[42] J.L. Falconer, R.J. Madix, J. Catal. 48 (1977) 262.
[43] M. Polanyi, E. Wigner, Z. Phys. Chem. 139 (1928) 439.
[44] P.A. Redhead, Vacuum 12 (1962) 203.
[45] E.G. Seebauer, L.D. Schnidt, Chem. Phys. Lett. 123 (1986) 129.
[46] B. Poelsema, G. Mechtersheimer, G. Comsa, Surf. Sci. 111 (1981) L728.
[47] R.J. Madix, G. Ertl, K. Christmann, Chem. Phys. Lett. 62 (1979) 38.
[48] E.A. Carter, B.E. Koel, Surf. Sci. 226 (1990) 339.
[49] B.E. Koel, D.A. Blank, E.A. Carter, J. Molec. Catal. A 131 (1998) 39.